Articles

Fluid-structure interaction analysis on shunt murmur generation mechanism of artificial angiostenosis model

NAKANE Noriaki[1], SASAKI Kazuma[2], OKU Tomoko[3], YAMAUCHI Shinobu[3], MOTOHASHI Yuka[3], SATO Toshio[*] and AGISHI Tetsuzo[4]

I. Introduction

In blood purification therapy, surgical anastomosis is performed between an artery and vein to draw blood outside the body and create vascular access (VA). At the VA point, arterial blood flows forcefully from the artery to the vein, showing different hemodynamics than usual blood flow. Furthermore, frequent punctures thicken the vascular intima, causing stenosis with a smaller blood vessel caliber.

One method for assessing VA function is auscultation of the shunt murmur. VA blockage and stenosis can be detected by listening to the shunt murmur. VA blockage is easily diagnosed by the disappearance of the shunt murmur. However, it has been pointed out that accurate diagnosis of the progression of stenosis from the shunt murmur is dependent on the skills and experience of or other subjective diagnosis by dialysis staff, and this method lacks quantification and objectivity. There is, therefore, a need to establish clear VA function assessment standards based on changes in the shunt murmur.Shunt murmurs are said to result from the jets arising from the rapid flow of a large volume of blood through the area of the arteriovenous anastomosis or stenotic lesion of the VA or from vibrations of the vascular wall arising as turbulent flow caused when the jet hits the vascular wall. A shunt murmur is closely related to factors such as flow rate through the VA and the shapes of the blood vessel and the stenosis. When the VA is in good condition, we hear low-pitch shunt murmurs consisting mainly of continuous, low-frequency components. When the condition of the VA worsens, this is replaced with high-pitch shunt murmurs consisting mainly of intermittent, high-frequency components. Few studies have been conducted to theoretically clarify the relationship between the condition of the VA stenosis and the characteristics of the shunt murmur that change with the VA condition. We are therefore investigating a method for theoretical assessment of the shunt murmur generation mechanisms and changes in shunt murmur characteristics accord-

[*] SATO Toshio: Professor, Graduate School of Engineering; Faculty of Biomedical Engineering, Toin University of Yokohama. 1614, Kurogane-cho, Aoba-ku, Yokohama 225–8503, Japan
[1] NAKANE Noriaki: Visiting researcher, Graduate School of Engineering, Toin University of Yokohama
[2] SASAKI Kazuma: Graduate school of Engineering, Toin University of Yokohama
[3] OKU Tomoko, YAMAUCHI Shinobu and Motohashi Yuka: Lecture, Faculty of Biomedical Engineering, Toin University of Yokohama
[4] AGISHI Tetsuzo: Professor Emeritus of Tokyo Women's Medical University

ing to stenosis condition. In our previous research, we carried out simulation tests using artificial angiostenosis models. For the simulation tests, we constructed artificial angiostenosis models that simulate stenosis by inserting acrylic cylindrical blocks with holes cut out of the center into silicone tubes simulating blood vessels. We then used a multifunctional pulsatile pump to create a pulsatile flow of water through the model. An acceleration sensor was attached to the surface of the silicone tube downstream of the cylindrical block made to simulate a stenosis, and simulated shunt murmur signals were measured. In this simulation test, the stenosis rate can be easily changed, allowing us to see how the frequency characteristics of the shunt murmur change with different stenosis rates and to visualize the flow through the artificial blood vessels with particle image velocimetry (PIV). From this information, we can quantitatively determine the effects of jets, turbulence, and eddies downstream of the stenosis on vibrations on the vascular wall. However, the shape of the VA in actual hemodialysis patients is complex, and it is not time- and cost-effective to attempt to recreate shunt murmurs by creating numerous stenosis models while changing the parameters such as stenosis shape and location according to each patient's individual VA condition. The creation of numerical analysis models from VA shape obtained as numerical data from computed tomography (CT) and magnetic resonance imaging (MRI) is now easy, and such models can be freely edited on CAD software to easily create numerical analysis models that simulate the VA conditions of different hemodialysis patients. It may therefore be possible to recreate shunt murmurs under various VA conditions by theoretically calculating shunt murmurs using numerical analysis. We attempted to conduct fluid-structure interaction analysis to theoretically calculate the shunt murmur of the different conditions of stenosis that exist, and we investigated the usefulness of numerical analysis

in the assessment of VA function.

II. Fluid-structure interaction analysis to calculate shunt murmur theoretically

2-1. Equations and calculation method used for analysis

To theoretically calculate the flow of water through an artificial angiostenosis model, the equation of continuity and the Navier-Stokes equations, which are dominant equations in fluid dynamics, were used. Incompressible flow was used to ensure that the flow velocity and the blood vessel deformation velocity were slow enough compared to the acoustic velocity. For calculations, the Finite Volume Method (FVM) and ANSYS CFX, a multiphysics analysis tool, were used.

$$\nabla u = 0 \quad \cdots\cdots\cdots\cdots\cdots\cdots\cdots\cdots (1)$$

$$\frac{\partial u}{\partial t} + u \nabla u = -\frac{1}{\rho} \nabla u + \frac{\mu}{\rho} \nabla^2 u \quad \cdots (2)$$

To structurally analyze the blood vessel vibrations, *i.e.* the deformations, a dynamic, generalized equation of motion was used. As the calculation method, the Finite Element Method (FEM) and ANSYS Mechanical, a multiphysics analysis tool, were used.

$$m \frac{\partial^2 x}{\partial t^2} + c \frac{\partial x}{\partial t} + kx = F \quad \cdots\cdots\cdots\cdots (3)$$

Fluid-structure interaction analysis is a calculation method in which the pressure calculation results obtained in fluid calculation are defined as the boundary conditions for structural calculations, and the volume of deformation obtained in structural calculations is defined as the boundary condition for fluid calculations. Calculations are repeated until the volume of change in each iterative calculation of each time falls below the criteria (converges). When the calculations converge, we move on to the next time step and continue the calculations until they converge again.

2-2. Numerical analysis model

A 10-mm-long acrylic artificial stenosis with an inner diameter of 4.8 mm (80% stenosis rate) and an outer diameter of 6-mm was inserted into a 1-mm-thick, 270-mm-long silicone tube with an inner diameter of 6 mm to create an artificial angiostenosis model. The area around the stenotic part appears as shown in *Fig.1*, with the left side upstream and the right side downstream.
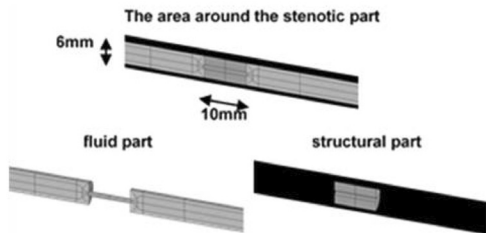

Fig.1 Numerical analysis model

2-3. Physical properties defined for calculation

Structural part

Artificial blood vessel model (material: silicone tube)

Mass density: 1230 kg/m^3

Young's modulus: 3.37 MPa (modulus of longitudinal elasticity)

Poisson's ratio: 0.45

Structural part

Stenotic part (material: acrylic)

Mass density: 1350 kg/m^3

Young's modulus: 3.2 GPa (modulus of longitudinal elasticity)

Poisson's ratio: 0.45

Fluid part

Water

Mass density: 997 kg/m^3

Viscosity coefficient: 8.899×10^{-4} Pa·s

Actual values were used for the mass density and Young's modulus of the structural parts, and representative values calculated from the literature were used for Poisson's ratio. Representative values defined in ANSYS CFX were used for the mass density and viscosity coefficient of the fluid part.

2-4. Boundary conditions

Structural parts

Inlet end: completely fixed in place

Outlet end: completely fixed in place

Interior: Pressure obtained in fluid calculations

Exterior: No settings

Fluid part

Inlet part: Maximum 140 mmHg, minimum 80 mmHg, fluctuating pressure at 60 times per minute

Outlet part: Constant pressure of 0 mmHg

Peripheral part: Wall boundary (velocity = 0)

Displacement obtained from structural calculations

Simulation tests under the same conditions were also conducted as an analysis to test the reliability of the numerical analysis results. The test apparatus is shown in *Fig.2*. The flow rate though the pulsatile pump was adjusted while monitoring the pressure in the inlet and outlet part on the bio-
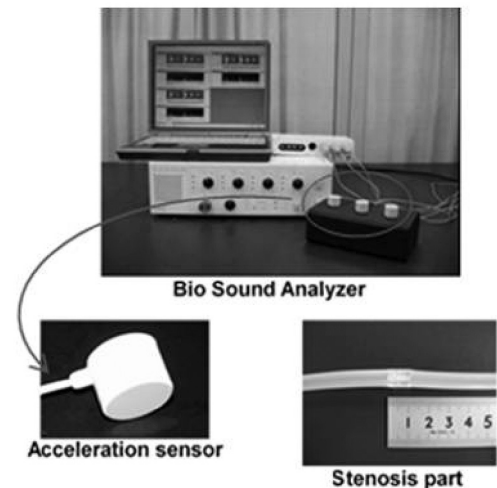

Fig.2 Test apparatus

logical information monitor.

In the simulation test, the outlet side was exposed to the atmosphere, so the pressure was set to 0 mmHg as the boundary condition for calculation. However, since there was a separation between the outlet part of the calculation area and the actual part that was exposed to the atmosphere, the pressure at the outlet part of the calculation area did not reach 0 mmHg, and the pressure was observed to change with the pulses from the pump. To account for this, a pressure resistance model incorporated in ANSYS CFX was used for calculation.

The pressure resistance is shown with the following formula.

$$\frac{\Delta p}{\delta} = \frac{\mu}{K_{perm}}|u| + K_{loss}\frac{\rho}{2}u^2 \quad \cdots\cdots\cdots\cdots (4)$$

Here, Δp is the pressure lost in the fluid resistance model, δ is the length of the fluid resistance model part, K_{perm} is the permeability coefficient obtained using Darcy's law, and K_{loss} is the pressure loss coefficient obtained using the Darcy-Weisbach equation. Each coefficient was calculated in the simulation test, and the pressure in the outlet part was measured at different flow rates. K_{perm} and K_{loss} were derived by approximating the results with quadratic equations.

In this calculation, the length of the fluid resistance model part δ was set to 20 mm, giving $\delta \mu/K_{perm}$ = 446785 [kg/m^3 s], and $\delta K_{loss} \rho/2$ = 1.92135×10^6 [kg/m^{4}]. As shown in **Fig.3**, the fluid resistance model was set in the downstream part of the fluid part of the calculation model.

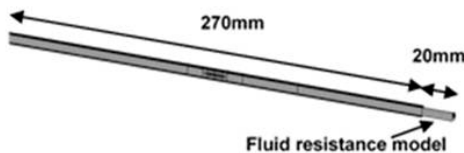**Fig.3** Fluid resistance model

III. Calculation results and discussion

3-1. Flow vectors of the stenotic part periphery

Fig.4 shows the flow vectors when the input pressure is 140 mmHg, equivalent to the systolic phase of the heart, and the flow vectors when the input pressure is 80 mmHg, equivalent to the diastolic phase of the heart. The flow vectors were obtained from visualization of the flow downstream of the stenosis recorded with PIV in the simulation test.
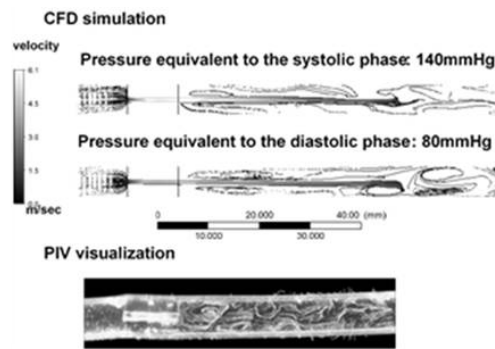

Fig.4 Visualization of velocity vector

You can see that jets formed downstream of the stenotic part in both the systolic and diastolic phases of the heart, and that the water flowed forcefully from the outlet of the stenotic part to the point about 50-mm downstream. You can also see that eddies that formed around the jet hit the vascular wall. The flow rate increased and decreased in places, and the spatial scale of the eddies was small, showing that the flow was extremely turbulent.

Further than 50 mm from the outlet of the stenotic part, the speed of the jets decreased rapidly. Low speed eddies formed, but there was little variation in speed in different areas, and the spatial scale of the eddies was large.

3-2. Vibrations of the artificial blood vessel wall

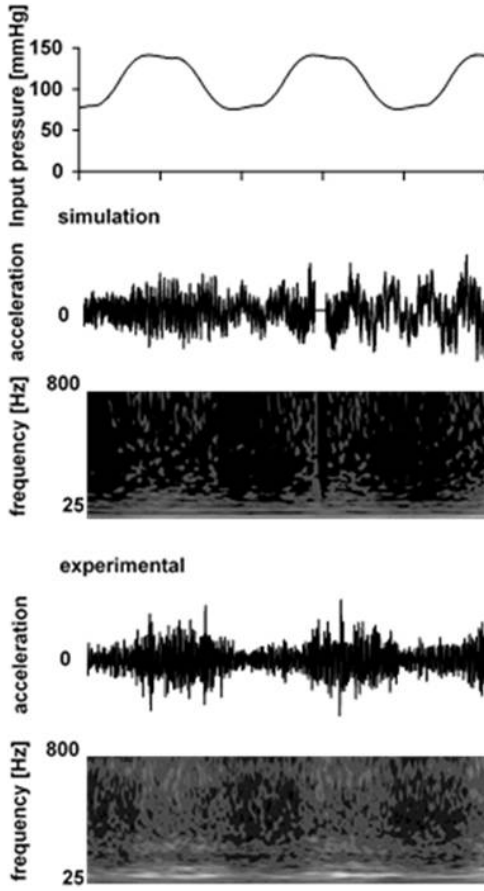**Fig.5** and **Fig.6** show the vibrations in the vas-
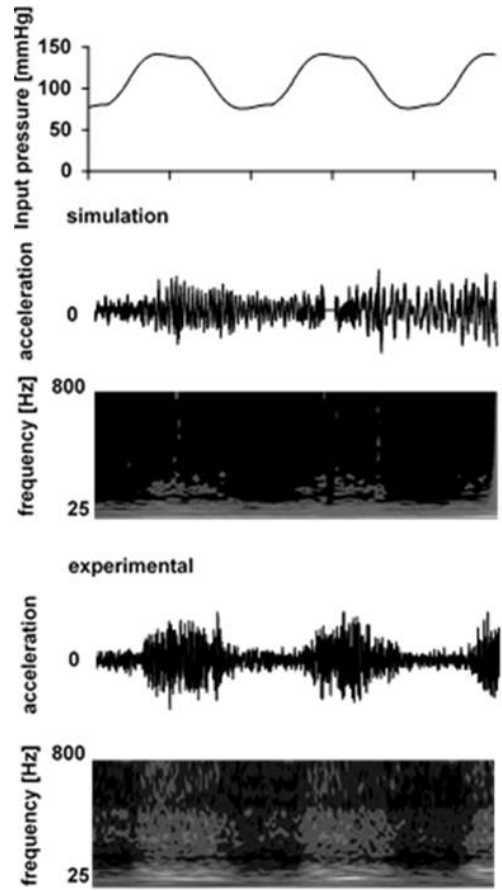
Fig.5 20-mm downstream

Fig.6 100-mm downstream

cular wall. **Fig.5** shows the results of analysis 20-mm downstream from the center of the stenosis, and **Fig.6** shows the results of the analysis 100-mm downstream from the center of the stenosis.

The first graph shows the input pressure waveform, the second and third show the acceleration in the numerical analysis and wavelet transformation results, and the fourth and fifth show the acceleration in the simulation test and the wavelet transformation results. The results are shown for 2.5 seconds. The color map of the wavelet transformation results image shows the size of the amplitude spectrum for each frequency component increasing from black to white.

Although the acceleration amplitude does not change greatly with fluctuating pressure 20-mm

downstream from the center of the stenotic part, you can see that the high-frequency components are larger in the systolic phase (high pressure part) than in the diastolic phase (low pressure part). High-frequency components are also intermittently detected from the wavelet transformation results, and these may correspond to the high-pitch shunt murmur heard when VA function declines.

In comparison, 100-mm downstream from the center of the stenotic part, you can see that the size of the acceleration amplitude changes with fluctuating pressure, and that the amplitude is larger in the systolic phase than in the diastolic phase. However, while the high-frequency components are larger in the systolic phase than in the diastolic phase, the difference is not as large as that

observed at the point 20-mm downstream. This suggests that it becomes more difficult to detect a high-pitch shunt murmur with distance from the stenotic part.

The reason for the spatial difference in the shunt murmur may be the flow generated downstream of the stenotic part. As mentioned above, the flow immediately after the stenotic part is very turbulent due to jets and changes greatly over a short time. The action of this flow hitting the vascular wall may generate a high-pitch shunt murmur with primarily high-frequency components. In contrast, the flow further away from the stenotic part is still turbulent, but the variability in the flow is not as large as the spot just past the stenotic part. For this reason, although the flow does hit the vascular wall, it may not be as intense as the area near the stenosis.

Proof of this can be seen in the temporal changes in pressure at the surface of the vascular wall obtained in the numerical analysis shown in **Fig.7**. The second and third graphs show the pressure against the surface of the vascular wall and the wavelet transformation results 20-mm downstream from the center of the stenosis, and the fourth and fifth graphs show the pressure against the surface of the vascular wall and the wavelet transformation results 100-mm downstream from the center of the stenosis. The pressure variation in the graph shows that the high-frequency components are larger 20-mm downstream than 100-mm downstream. The high-frequency components may have caused larger deformations on the vascular wall surface 20-mm downstream compared to 100-mm downstream.

The high-frequency component vibrations on the vascular wall were smaller in the results obtained by numerical analysis than in the test results. This may have been due to differences in the definitions of physical properties and boundary conditions in the numerical analysis compared to the test. In particular, in the simulation test, the
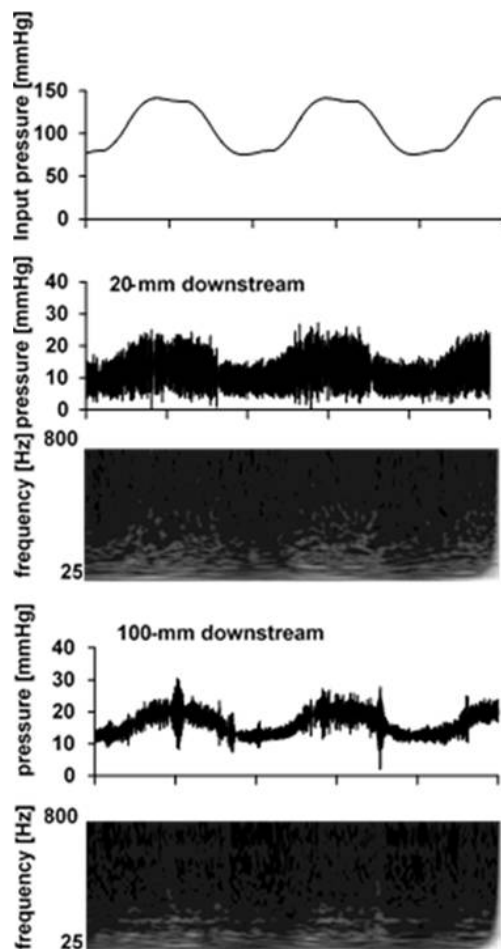

Fig.7 Pressure at surface of vascular wall

area around the vascular wall was covered with a biological phantom (konjak) based on clinical trials to simulate the skin and muscles in a dialysis patient. This suppressed low-frequency vibrations of the artificial blood vessel and allowed for relatively larger high-frequency components. This effect was not considered in the numerical analysis, and low-frequency components around 30 to 40 Hz were consistently present. Since these low-frequency components were always present in the numerical analysis, they were likely the natural vibrations arising from fixing the vascular wall inlet and outlet sides in place. For quantitative assessment using numerical analysis, it may be necessary to add a condition simulating the skin

or muscles on the vascular wall part to the current boundary conditions.

4. Summary and further studies

In the present study, we formed the following conclusions from the results of an attempt to calculate the shunt murmur of an artificial blood vessel containing a stenotic part with a stenosis rate of 80% using fluid-structure interaction analysis.

1) Jets form downstream of the stenotic part, and the flow becomes very turbulent from those jets.
2) The vascular wall vibrates strongly just past the stenosis where the jets are forceful, generating a high-pitch shunt murmur.
3) Although the sizes of vibrations of high-frequency components varied with the different boundary conditions between the numerical analysis and simulation tests, the flow and the intermittent nature of the vibrations were qualitatively consistent, confirming the usefulness of numerical analysis.

We plan to conduct further studies revising the boundary conditions and making comparisons with simulation tests using different shapes to theoretically examine the shunt murmur generation mechanisms.

[References]

1) Sasaki Kazuma, Motohashi Yuka, Yamauchi Shinobu, Sato Toshio and Agishi Tetsuzo: "Experimental study of shunt murmur generating mechanism based on flow visualization of pseudo angiostenosis model": Research Bulletin No.30 June 2014 Toin University Of Yokohama, pp.137–145

2) S.W. Lee, P.F. Fischer, F. Loth, T.J. Royston, J.K. Grogan, H.S. Bassiouny: "Flow-induced vein-wall vibration in an arteriovenous graft": Journal of fluids and structures, April 2005

3) Nakane Noriaki, Sasaki Kazuma, Oku Tomoko, Yamauchi Shinobu, Motohashi Yuka, Sato Toshio and Agishi Tetsuzo: "Usability of numerical computation about mechanism of generating shunt murmur": 14th Toin International Symposium on Biomedical Engineering, November 2019 pp.114–115